The "shallow-waterness" of the wave climate in European coastal regions

Kai Håkon Christensen[1], Ana Carrasco[1], Jean-Raymond Bidlot[2], and Øyvind Breivik[1]

[1]Norwegian Meteorological Institute, Henrik Mohns plass 1, N-0313 Oslo, Norway
[2]European Centre for Medium Range Weather Forecasts, Shinfield Park, Reading, RG2 9AX, UK

Correspondence to: Kai H. Christensen (kaihc@met.no)

Abstract. In contrast to deep water waves, shallow water waves are influenced by bottom topography, which has consequences for the propagation of wave energy as well as for the energy and momentum exchange between the waves and the mean flow. The ERA-Interim reanalysis is used to assess the fraction of wave energy associated with shallow water waves in coastal regions in Europe. We show maps of the distribution of this fraction as well as time series statistics from 8 selected stations. There is a strong seasonal dependence and high values are typically associated with winter storms, indicating that shallow water wave effects can occasionally be important even in the deeper parts of the shelf seas otherwise dominated by deep water waves.

1 Introduction

The purpose of this brief note is to present some aspects of ocean surface waves related to bottom topography. If the wavelength is small compared to the local water depth, the waves are unaffected by the presence of the sea floor and the wave energy balance is dominated by input from wind, dissipation by wave breaking and white capping, and nonlinear wave-wave interactions. If the wavelength is large compared to the local water depth, the situation is quite different and the wave energy propagation will directly depend on the bottom topography, with implications for dissipation and sediment transport in the bottom boundary layer, wave-mean flow interactions through wave radiation stresses, modification to the nonlinear wave-wave interactions, and so on (e.g., Komen et al., 1994; Smith, 2006).

The main aim of this study is to identify in which coastal regions in Europe shallow water wave effects may be important and to quantify the fraction of wave energy associated with ocean waves that can "feel" the bottom. As such, this note differs from previous studies that focus on the wave climate, employing either hindcasts (e.g., Gorman et al., 2003; Dodet et al., 2010; Reistad et al., 2011; Aarnes et al., 2012), reanalyses (e.g., Dee et al., 2011; Reguero et al., 2012) or climate projections (e.g., Wang et al., 2004; Hemer et al., 2013) to assess average and/or extreme values of typical wave parameters on regional or global scales. Typical wave conditions can be classified according to the shape of the two-dimensional wave spectrum (e.g., Boukhanovsky et al., 2007), utilizing the fact that the waves will often be a combination of remotely forced swell and locally generated wind waves. In coastal regions, a significant proportion of the wave energy may be associated with waves on intermediate depth, and at any specific location this proportion will vary in time due to variations in the local and remote

forcing of the waves. It should be emphasized that we do not make a clear distinction here between intermediate and shallow water waves, for which the wavelength is much larger than the local depth. Our analysis is based on separating the wave spectra into high and low frequency parts using a prescribed, depth-dependent frequency threshold.

The outline of this paper is as follows: In Sec. 2 we introduce the analysis methods and reanalysis data, while in Sec. 3 we
5   present the results. A brief discussion and some concluding remarks are given in Sec. 4.

2   Concept and methods

The analysis is quite simple: we divide the wave spectrum into high and low frequency parts, using prescribed values of the ratio n between the wave group and phase velocities to identify the frequency that separates the two parts. The wave energy in the low frequency part is divided by the total wave energy, and maps and time series statistics of this ratio are presented. Since
10 wave dispersion depends on the local water depth in shallow waters, the frequency limit for any given n will vary in space. The data are obtained from the wave model component of the ERA-Interim reanalysis (Dee et al., 2011).

2.1   Wave dispersion

The dispersion relation for surface gravity waves is

$$\omega^2 = gk \tanh kh. \tag{1}$$

15 Here ω is the wave angular frequency, g is the acceleration due to gravity, k is the wave number, and h is the water depth. The phase velocity c in the direction of wave propagation is $c = \omega/k$. The group velocity is given by $c_g = d\omega/dk$, and using (1) we have

$$n \equiv \frac{c_g}{c} = \frac{1}{2} + \frac{kh}{\sinh 2kh}. \tag{2}$$

The ratio n between the group and the phase velocity is thus a function of the local water depth and the wave number. The
20 limiting cases are for deep water ($kh \to \infty$), when $n = 1/2$, and for shallow water ($kh \to 0$), when $n = 1$ and the waves are non-dispersive. If $n > 1/2$, the waves are thus to some extent influenced by the bottom. In the present study we will consider n-values of 0.55, 0.65, 0.75 and 0.85. We will classify the waves according to their frequency $f = \omega/2\pi$, and for any given value of n the corresponding frequency f_n can be obtained from (1) and (2). To investigate the "shallow-waterness" of a certain location we compute the ratio of energy of the waves that feel the bottom to the total energy:

25 $$r_n = \frac{\int_0^{2\pi} \int_0^{f_n} F \, df \, d\theta}{\int_0^{2\pi} \int_0^{\infty} F \, df \, d\theta}, \tag{3}$$

where $F(f, \theta)$ is the directional wave spectrum obtained from the reanalysis data.

2.2   ERA-Interim wave spectra

ERA-Interim (ERA-I) is a global coupled atmosphere-wave-ocean reanalysis starting in 1979 (Dee et al., 2011). An irregular latitude-longitude grid ensures relative constancy in atmospheric grid resolution towards the poles. T255 is the Gaussian grid

Name	Latitude	Longitude	Depth [m]
LF3J	61.20	2.30	181
62069	48.29	-4.97	137
62023	51.40	-7.90	103
AUK	56.39	2.05	79
LF5U	56.50	3.21	60
K13	53.20	3.22	29
EURO	51.99	3.27	28
BSH03	54.00	8.12	20

Table 1. List of stations.

with a spacing of the order 80 km, but atmospheric parameters are also made available (following bi-linear interpolation) on a 0.75x0.75 degree regular lat-lon grid. The model and data assimilation scheme of the reanalysis are based on Cycle 31r2 of the Integrated Forecast System (IFS). The wave model WAM is coupled to the atmospheric part of the IFS through the exchange of the Charnock parameter. See Janssen (1989, 1991, 2004) for details of the coupling and Dee et al. (2011) for an overview of the ERA-Interim reanalysis. The resolution of the wave model model component is $1.0°$ on the Equator but the resolution is kept approximately constant globally through the use of a quasi-regular latitude-longitude grid where grid points are progressively removed toward the poles (Janssen, 2004). The spectral range from 0.035 to 0.55 Hz is spanned with 30 logarithmically spaced frequency bands. The angular resolution is $15°$ (24 bins). Full two-dimensional spectra are archived every six hours on the native grid. The ERA-I WAM implementation incorporates shallow-water effects important in areas like the southern North Sea (Komen et al., 1994). ERA-I also uses a subgrid scheme to represent the downstream impact of unresolved islands (Bidlot, 2012).

2.3 Stations

In addition to presenting maps of the ratio r_n, we analyse eight stations in some detail using the six-hourly time series from ERA-I. The station names, positions and depths are listed in Table 1, and the positions are also shown in Fig. 1. These stations correspond to locations with wave observations, and we have focused on the European Northwest Shelf Sea where shallow water waves are most prominent. Three stations southwest of Ireland and the UK, and in the northern North Sea are exposed to long swell from the North Atlantic (62023, 62069 and LF3J), and all these stations are in relatively deep water (103 m, 137 m, and 181 m, respectively). Two stations are in intermediate depths in the middle of the North Sea (AUK and LF5U), while the rest are in the shallow southern part of the North Sea.

3 Results

We first investigate the spatial distribution of n. For this purpose we use monthly averages of the wave spectra. We then investigate the temporal variation of n at the eight stations defined in Sec. 2.3, presenting monthly median values as well as the 5th, 25th, 75th and 95th percentiles. Finally, we plot n-values against mean period and significant wave height to investigate the variation of n with wave steepness.

3.1 Spatial distribution

Values of r_n are typically highest in the period December-March and Fig. 2 shows maps of the average values of r_n for January for the period 1979-2012. Unsurprisingly, the highest values are found in shallow waters, including the North Sea, southwest of Ireland and UK, south of Spitsbergen, in the eastern part of the Barents Sea, and in the central Mediterranean. The monthly average r_n ratios become, by necessity, smaller for increasing n, and is for $n = 0.85$ vanishingly small everywhere.

3.2 Seasonal dependence

Figures 3-4 show monthly values of significant wave height (H_s), mean period (T_{m2}), and r_n for the eight stations listed in Table 1. The data are presented as median values and the 5th, 25th, 75th and 95th percentiles for the period 2003-2013. Significant wave height and mean periods are highest in the winter months, and the spread is also larger. The values of r_n are quite small for the three stations with largest depth, but we also see e.g. values of $r_{0.65}$ reaching 15% at station 62023 (103 m depth). Notably the $r_{0.65}$ values are lower for the shallower AUK station (79 m depth), which is explained by this station being sheltered from the long swell originating in the North Atlantic. The r_n values are consistently lower in the summer months.

3.3 Dependence on wave steepness

Finally we investigate if high r_n values are associated with a particular sea state, and Figs. 5-6 show scatter plots of all the data points in a H_s/T_{m2} diagram. We only consider $n = 0.55$. For the deepest station LF3J there are only a few cases with relatively high $r_{0.55}$ values (to put this in context: there are over 16000 data points altogether). For the rest of the stations it is clear that $r_{0.55}$ is primarily correlated with the mean period, and not with the significant wave height, and high values can be found both for high and low waves. There is a lower limit to the mean period that increases with the wave height, however, hence the average value of $r_{0.55}$ in general increases with H_s.

4 Conclusions

Data from the wave model component of the ERA-Interim reanalysis have been used to quantify the "shallow-waterness" of the wave climate in coastal regions in Europe. The "shallow-waterness" is here defined as the ratio r_n of wave energy of the components that are influenced by the bottom compared to the total wave energy. As can be expected, the ratios are largest

during winter and on the European Northwest Shelf. Eight stations over that area have therefore been investigated in more detail.

This work has a bearing on coupled wave-ocean modeling systems, for example, shallow water wave-induced radiation stresses give rise to barotropic forcing terms that can play a role for storm surge modeling. With the exception of the shallowest

5   parts of the shelf seas, the "shallow-waterness" is on average quite small, but occasional high values of r_n can be found in intermediate water depths (~ 100 m). Destructive storm surge events are typically caused by intense winter storms with high waves, and our results suggest that in such situations shallow water effects can be important even at great distances from the coast. The "shallow-waterness" is primarily correlated with the mean period and can be found for both high and low waves, but shallow water effects become increasingly important for higher waves since these are associated with longer mean periods.

10   *Acknowledgements.* This work was funded by the European Union Seventh Framework Program FP7/2007-2013 under grant no 283367 (MyOcean2). Ø.B. was partly supported by the European Union FP7 project MyWave (grant no 284455) and in part by the ExWaMar project funded by the Research Council of Norway.

References

Aarnes, O. J., Breivik, Ø., and Reistad, M.: Wave Extremes in the Northeast Atlantic, J. Climate, 25, 1529–1543, doi:10.1175/JCLI-D-11-00132.1, 2012.

Bidlot, J.-R.: Present status of wave forecasting at ECMWF, in: Workshop on Ocean Waves, 25-27 June 2012. Available online at
5   http://www.ecmwf.int/publications/, 2012.

Boukhanovsky, A. V., Lopatoukhin, L. J., and Guedes Soares, C.: Spectral wave climate of the North Sea, Appl. Ocean Res., 29, 146–154, doi:10.1016/j.apor.2007.08.004, 2007.

Dee, D., Uppala, S., Simmons, A., Berrisford, P., Poli, P., Kobayashi, S., Andrae, U., Balmaseda, M., Balsamo, G., Bauer, P., P, B., Beljaars, A., van de Berg, L., Bidlot, J., Bormann, N., et al.: The ERA-Interim reanalysis: Configuration and performance of the data assimilation
10   system, Q. J. Roy. Meteorol. Soc., 137, 553–597, doi:10.1002/qj.828, 2011.

Dodet, G., Bertin, X., and Taborda, R.: Wave climate variability in the North-East Atlantic Ocean over the last six decades, Ocean Model., 31, 120–131, doi:10.1016/j.ocemod.2009.10.010, 2010.

Gorman, R. M., Bryan, K. R., and Laing, A. K.: Wave hindcast for the New Zealand region: Nearshore validation and coastal wave climate, New Zeal. J. Mar. Fresh., 37, 567–588, doi:10.1080/00288330.2003.9517190, 2003.

15   Hemer, M. A., Fan, Y., Mori, N., Semedo, A., and Wang, X. L.: Projected changes in wave climate from a multi-model ensemble, Nat. Clim. Change, 3, 471–476, doi:10.1038/nclimate1791, 2013.

Janssen, P.: Wave-induced stress and the drag of air flow over sea waves, J. Phys. Oceangr., 19, 745–754, doi:10.1175/1520-0485(1989)019<0745:WISATD>2.0.CO;2, 1989.

Janssen, P.: Quasi-linear theory of wind-wave generation applied to wave forecasting, J. Phys. Oceangr., 21, 1631–1642, doi:10.1175/1520-
20   0485(1991)021<1631:QLTOWW>2.0.CO;2, 1991.

Janssen, P.: The interaction of ocean waves and wind, Cambridge University Press, Cambridge, UK, 2004.

Komen, G. J., Cavaleri, L., Donelan, M., Hasselmann, K., Hasselmann, S., and Janssen, P. A. E. M.: Dynamics and modelling of ocean waves, Cambridge University Press, Cambridge, 1994.

Reguero, B. G., Méndez, M., Méndez, F. J., Mínguez, R., and Losada, I. J.: A Global Ocean Wave (GOW) calibrated reanalysis from 1948
25   onwards, Coastal Engineering, 65, 38–55, doi:10.1016/j.coastaleng.2012.03.003, 2012.

Reistad, M., Breivik, Ø., Haakenstad, H., Aarnes, O. J., Furevik, B. R., and Bidlot, J.-R.: A high-resolution hindcast of wind and waves for the North Sea, the Norwegian Sea, and the Barents Sea, J. Geophys. Res., 116, 18 pp., doi:10.1029/2010JC006402, 2011.

Smith, J. A.: Wave Current Interactions in Finite Depth, J. Phys. Oceanogr., 36, 1403–1419, doi:10.1175/JPO2911.1, 2006.

Wang, X. L., Zwiers, F. W., and Swail, V. R.: North Atlantic Ocean Wave Climate Change Scenarios for the Twenty-First Century, J. Climate,
30   17, 2368–2383, doi:10.1175/1520-0442(2004)017<2368:NAOWCC>2.0.CO;2, 2004.
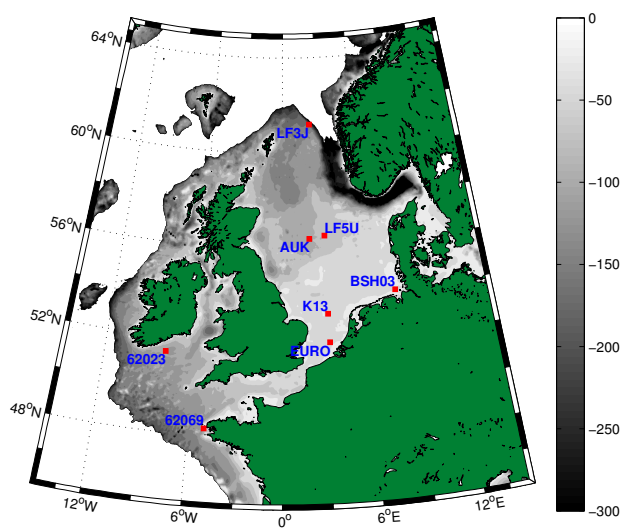
Figure 1. Map of station positions. Depths less than 300 meters are indicated in gray.
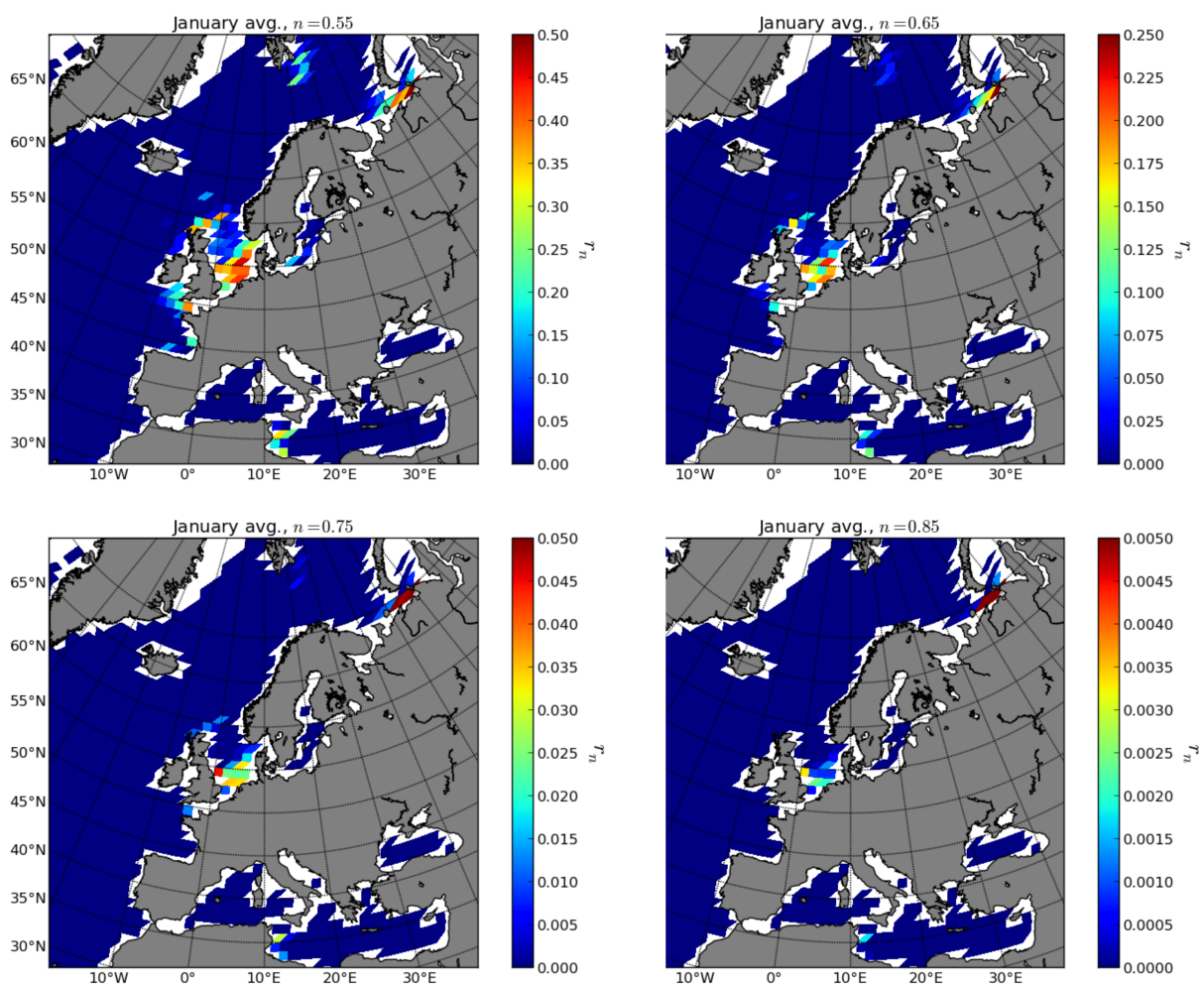
Figure 2. Average values of $r_{0.55}, r_{0.65}, r_{0.75}, r_{0.85}$ in January for the period 1979-2012.
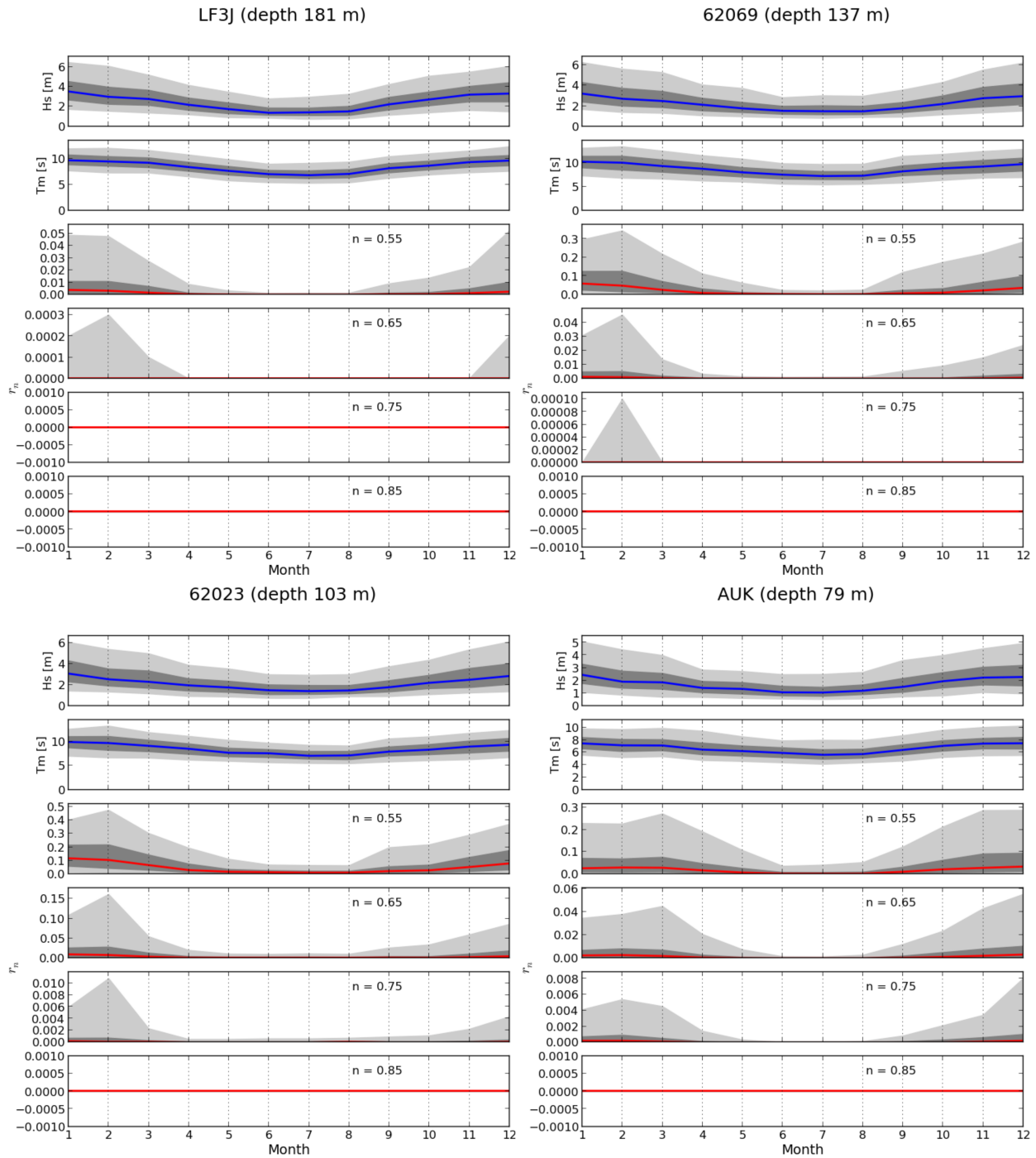
Figure 3. Monthly values of significant wave height, mean period, and r_n values for $n = 0.55$, 0.65, 0.75 and 0.85 at stations LF3J, 62029, 62023 and AUK. Median values are given by red and blue lines; 25th to 75th percentiles are shown as dark gray; 5th to 95th percentiles are shown as ligth gray.
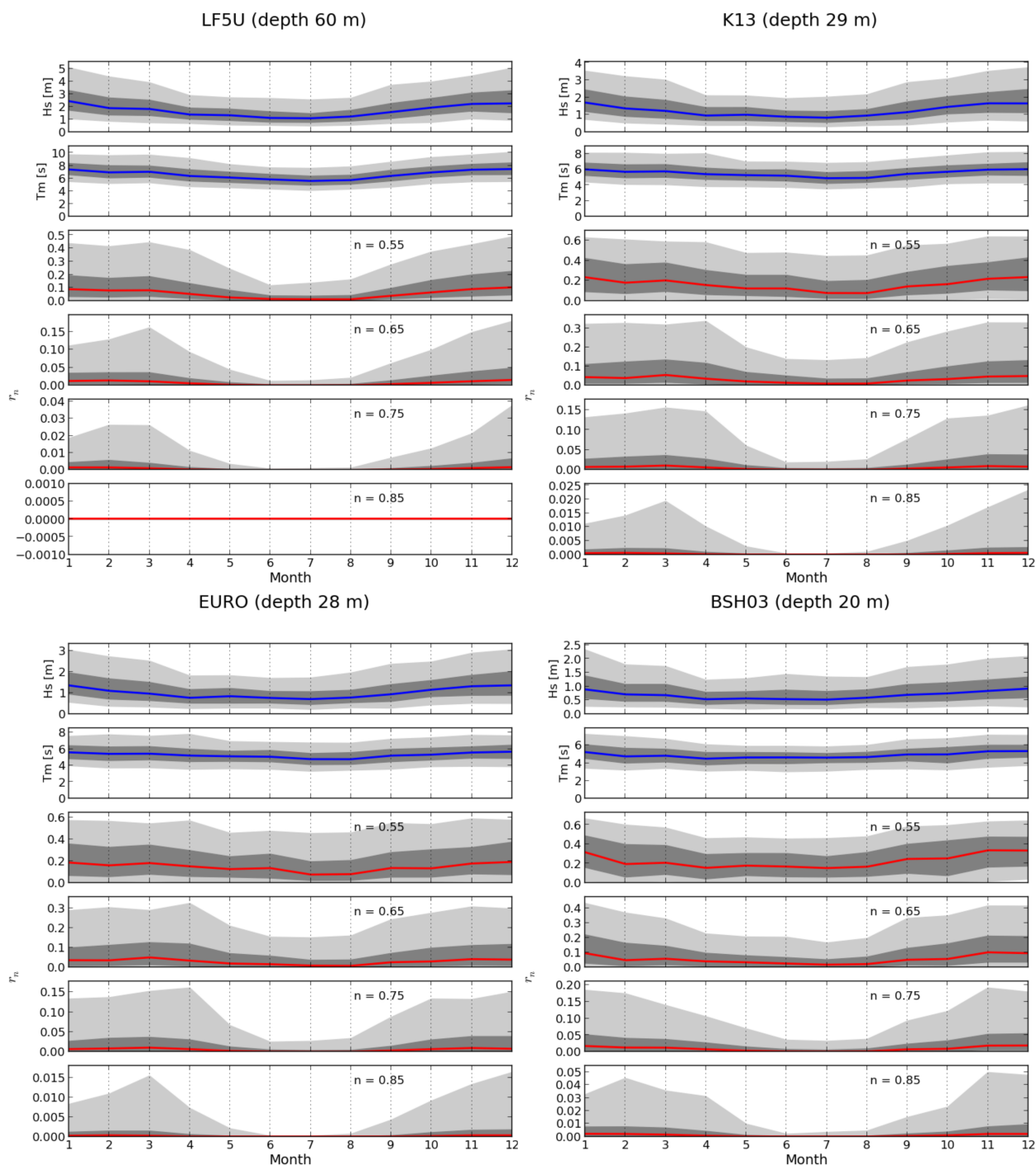
Figure 4. Same as Fig. 3, but for stations LF5U, K13, EURO and BSH03.
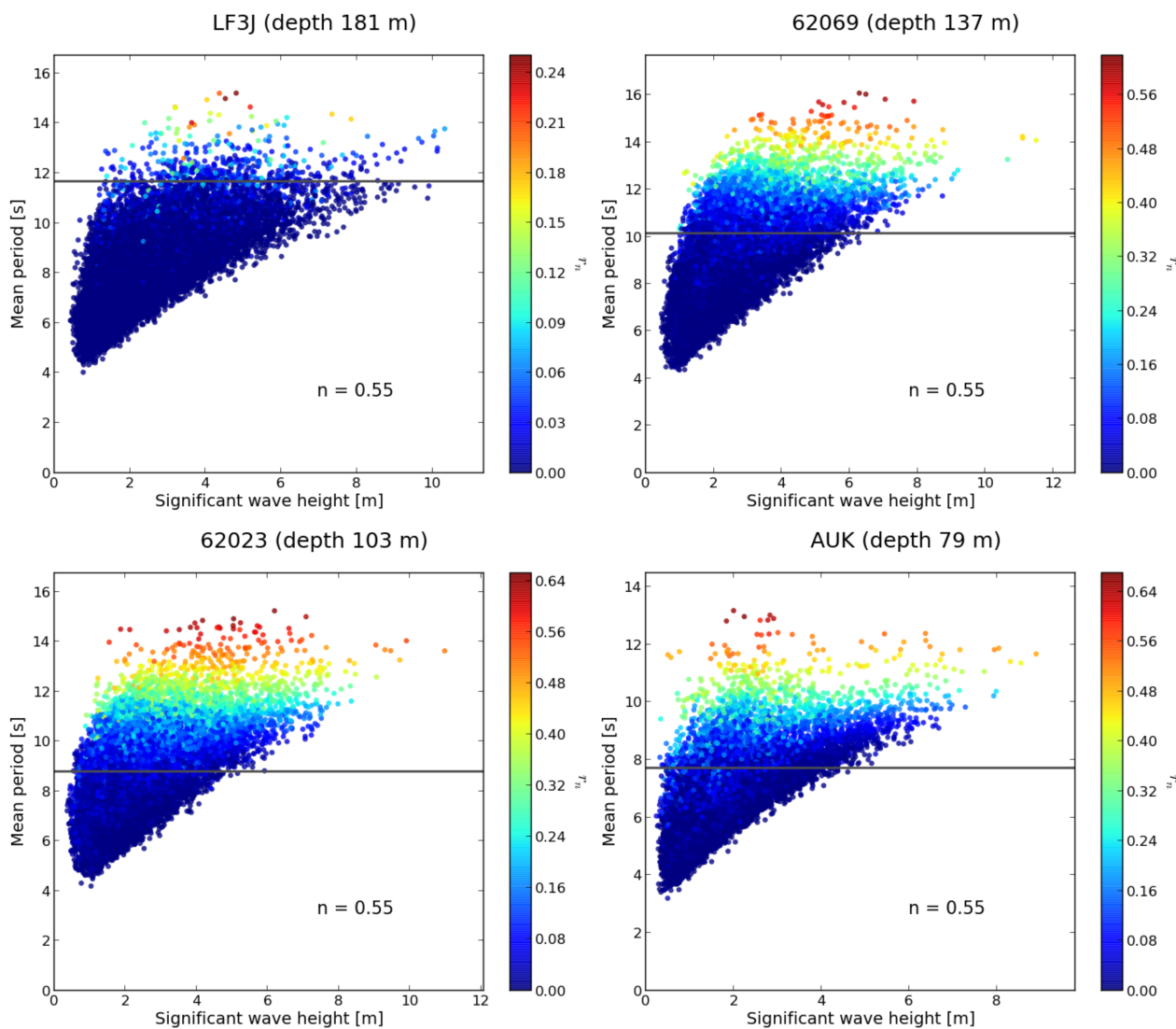
Figure 5. Scatter plot of all the data points for stations LF3J, 62029 62023 and AUK, with colors indicating $r_{0.55}$ values. The gray line indicates the period corresponding to $n = 0.55$ for each station.
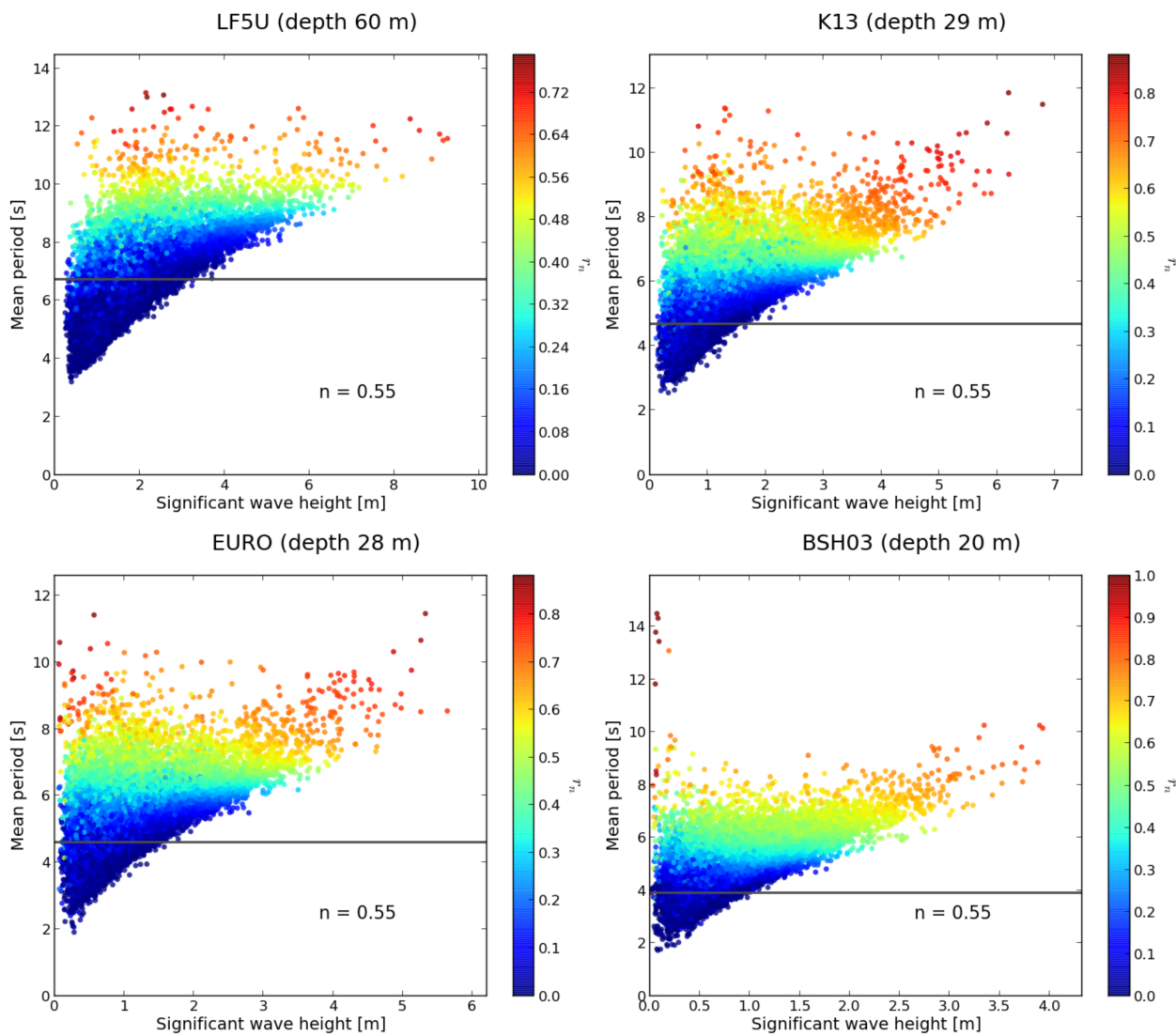
Figure 6. As Fig. 5, but for stations LF5U, K13, EURO and BSH03.